SLAC-R-756

A Preliminary Measurement of the Left-Right Parity-Violating ep Asymmetry at E158

Jed Biesiada

Undergraduate Honors Thesis at UC Berkeley

Stanford Linear Accelerator Center, Stanford University, Stanford, CA 94309

Work supported by Department of Energy contract DE–AC02–76SF00515.

A Preliminary Measurement of the Left−Right Parity−Violating *ep* Asymmetry at E158

Jedrzej Biesiada
UC Berkeley

Advisor: Yury Kolomensky
UC Berkeley

August 16, 2002

Submitted in Fulfillment of the Honors Graduation Requirement of the Physics Department at UC Berkeley and as a Technical Note for the E158 experiment

Abstract

This thesis investigates the parity−violating *ep* asymmetry based on the Run I data produced in Spring of 2002 by the E158 experiment , located at the Stanford Linear Accelerator Center. The main scientific objective of the experiment is the precision measurement of the weak mixing angle of the Standard Model. The *ep* asymmetry is an important background in the experiment and theoretically interesting in its own right, providing insights into the structure of the proton. The analysis centers upon identifying systematic error and consistency. The definite measurement of the *ep* asymmetry will await the final reprocessing of the data set during the Fall of 2002. A preliminary estimate of the *ep* asymmetry is

$$A_{ep}^{PV}(45\,GeV) = (-1.66 \pm 0.07(stat) \pm 0.14(syst))\ ppm$$
$$A_{ep}^{PV}(48\,GeV) = (-2.07 \pm 0.10(stat) \pm 0.17(syst))\ ppm$$

$$\frac{A_{ep}^{PV}(48\,GeV)}{A_{ep}^{PV}(45\,GeV)} = 1.25 \pm 0.08(stat) \pm 0.03(syst)$$

1. Theoretical Introduction

1.1 Electroweak force

The electroweak force is a fundamental interaction of nature. Along with the strong interaction it constitutes the gauge sector of the Standard Model, dictating the interactions of the particle section, which in turn is a categorization of the fundamental constituents of matter, leptons and quarks. Historically, the electroweak force arose out of the unification of electromagnetism and the weak interaction, the first successful theoretical formulation of which was composed by Weinberg, Salaam, and Glashow in 1967−70 [Wei 67; Sal 68; Gla 70]. It is fundamentally characterized by the SU(2) x U(1) Lie symmetry. This symmetry features four interaction fields, each mediated by a massless boson. The four bosons are a triplet W^+,W^0, and W^-, and a neutral B boson.

The fundamental symmetry is, however, broken below some characteristic symmetry−breaking energy scale. The symmetry−breaking mechanism endows the bosons with rest mass, effects a mixing of the W^0, B, and separates the interaction into two sectors, the electromagnetic sector and the weak sector. The physical electroweak bosons encountered at most experimentally accessible energy scales are the W^+, W^-, and Z^0, which are the weak mediators, and γ, the familiar photon of the electromagnetic

force. The Z^0 and γ bosons are linear combinations of the W^0 and B bosons in the original quadruplet. The W and Z^0 bosons have nearly the same masses of approximately 90 GeV, determined experimentally by the many experiments at CERN's LEP and Fermilab's Tevatron facilities. [Lep 01; Lep 93] The photon is massless.

The electroweak interactions are characterized by the couplings between the particles that carry electromagnetic and weak charge. In quantum field theory formalism, these couplings are modeled as currents. The W^+ and W^- are thus considered the charged current of the weak interaction, while the W^0 corresponds to the neutral weak current. However, since in the "real world" of low energy, empirically accessible regimes it is the Z^0 boson that is the neutral weak mediator, it is the degree of mixing between the W^0 and B that constitutes the weak neutral current. Its magnitude is:

$$J_{\lambda}^{NC} = J_{\lambda}^{W^0} - 4Qf \sin^2 \vartheta_W J_{\lambda}^{EM} \quad .$$

Here, J is the appropriate current for any given gauge sector; Q_f is the electric charge of an elementary fermion (lepton or quark); and θ_W is the Weinberg or weak−mixing angle, which characterizes the mixing between the weak neutral−current and electromagnetic gauge sectors. It is defined by

$$\sin^2 \vartheta_W = 1 - \frac{M_W^2}{M_Z^2} \quad ,$$

where M_W and M_Z, are the W and Z^0 masses, respectively.

In actual experimental interactions, the phenomenology of which is codified in reaction cross sections, rates, and various asymmetries, the weak mixing angle is

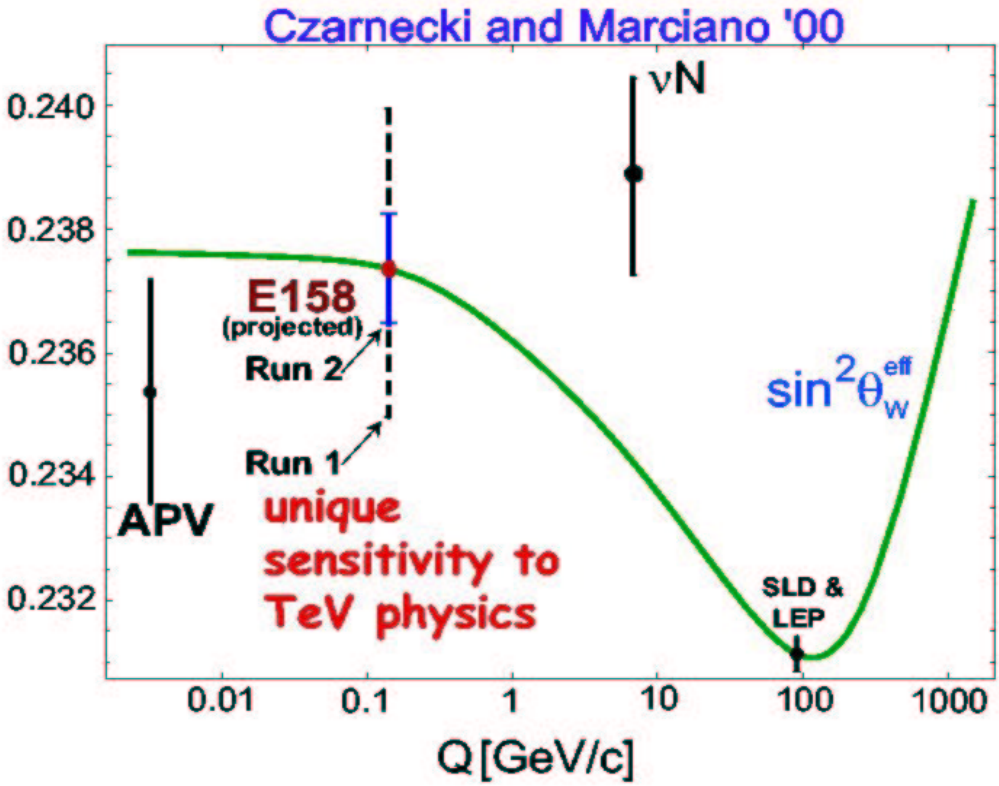

Figure 1. Standard Model running of the effective Weinberg Angle as compared with experimental results

redefined as the effective magnitude of mixing between the SU(2) and U(1) sectors. This "effective" weak−mixing angle is then dependent upon Q^2, defined as the negative of the square of the four−momentum transfer in a given collision. The dependence is a result of Q^2−dependent electroweak radiative corrections to the tree−level cross−section. (Fig. 1) In performing an experiment the observables of which are sensitive to the value of the weak mixing angle, one can determine whether $sin^2\theta_W^{eff}$ at a given Q^2 is indeed consistent with the running of the constant predicted by the Standard Model. A precise measurement of the Weinberg angle thus constitutes a rigorous test of the minimal SU(2) x U(1) electroweak model, up to the uncertainties involved with the determined W and Z^0 masses. The angle has been accurately measured at the Z^0 pole by several

experiments at LEP [Woods 95]. However, several experiments have obtained statistically significant deviations from the Standard Model at low Q^2. [NuT 01] The E158 experiment purports to determine the Weinberg mixing angle with unprecedented accuracy away from the Z^0 pole by a precise measurement of the left−right parity violating asymmetry in polarized electron−electron Møller scattering at $Q^2 = 0.03$ GeV^2.

1.2 Parity Violating Asymmetries in e^-e^- and ep Scattering

The phenomenon of parity violation is inherent in the weak interaction but does not occur in the electromagnetic interaction. The weak interaction couples preferentially to particle states of left chirality, while the electromagnetic coupling has no chiral prejudice. This preference can be detected in reactions mediated by the neutral weak current. However, most processes not involving neutrinos will be dominated by the electromagnetic interaction, which is seven orders of magnitude stronger than the weak interaction at $Q^2 = 0.03$ GeV^2. (The effective coupling is inversely proportional to the difference between Q^2 and the square of the mass of the bosonic mediator, which in the case of the Z^0 is $(90\ GeV)^2$.) Thus, in order to observe parity−violating neutral−current effects, one needs to observe quantum interference between the electromagnetic and weak neutral−current couplings, which is detectable, although still small compared to the purely electromagnetic, parity−conserving coupling.

In the E158 experiment, the Møller scattering of a polarized electron beam off of

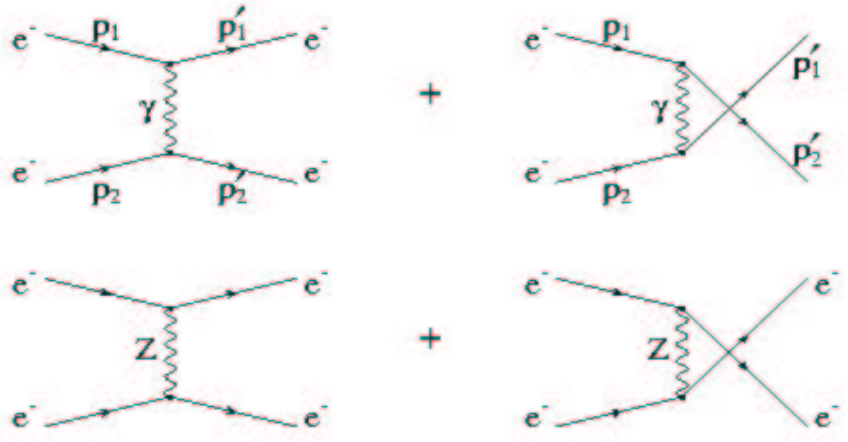

Figure 2. Neutral−current amplitudes leading to the tree−level left−right asymmetry

an unpolarized fixed−target electron is dominated by the leading tree−level Feynman diagrams shown in Figure 2. The interference between the EM and weak neutral current in Møller scattering produces an asymmetry between the scattering cross−sections of left− and right−polarized electron beams. The left−right asymmetry is defined by

$$A_{LR} = \frac{(\sigma_R - \sigma_L)}{(\sigma_R + \sigma_L)}$$

where σ is the appropriate measured scattering asymmetry. Using Feynman calculus on Figure 2, the theoretical asymmetry is

$$A_{LR} = mE \frac{G_F}{\sqrt{2}\pi\alpha} \frac{16 \sin^2\Theta}{(3+\cos^2\Theta)^2} \left(\frac{1}{4} - \sin^2\vartheta_W\right)$$

Here, E is the energy of the incident beam, G_F is the Fermi coupling constant, m is the electron mass, and Θ is the center−of−mass scattering angle. [Der 79] Hence, the left−

right asymmetry is directly related to the value of the weak−mixing angle.

Another process that occurs in E158 is electron−proton (*ep*) scattering, wherein the incident beam electron scatters off of a nuclear proton in the fixed target. The dynamics of this process are similar but complicated by the compositeness of the proton. The proton is a bound hadronic state composed of three valence quarks, two u quarks and one d quark, and a sea of quark−antiquark pairs, gluons, and other hadronic resonances. The state is bound by the strong interaction, which is characterized by the theory of Quantum Chromodynamics. At high Q^2 (> 1 GeV^2), the incident electron penetrates the proton and scatters off of the constituent particles (quarks or resonances). This process will be termed inelastic scattering, since the electron penetrates the proton. This regime is well understood, as QCD is tractable there since asymptotic freedom of the bound quarks allows for a standard perturbative treatment. At low Q^2 (< 0.01 GeV^2), the electron does not penetrate the proton but scatters coherently from the entire bound state. This will be called elastic scattering. Here, QCD is not at present computationally tractable, but the elastic scattering is nevertheless well understood by considering only hadronic degrees of freedom. In other words, the proton behaves as a point particle and the left−right asymmetry and other reaction quantities are similar to the corresponding quantities in electron−electron scattering. In the energetically intermediate case, which is the one relevant for this experiment (Q^2 = 0.03 GeV^2), the scattering is a superposition of elastic and inelastic interactions. From the point of QCD, this is a theoretically interesting energetic regime, as determining the fractional inelastic cross−section is relevant for the characterization of the proton's internal structure. It is this question that this paper will consider.

1.3 The Proton: Internal Structure

As the proton is a composite particle, its decomposition into constituent partons should in principle be entirely computable and analytical. Unfortunately, such a characterization has so far proven to be difficult and is at present theoretically uncertain. While this constitutes a theoretical incompleteness in QCD, it also establishes low−energy QCD as a live theoretical pursuit in physics, distinct from string theories which have come to dominate most sectors of the theoretical physics community. Experimental examinations of hadronic structure are an important stimulus and guidepost for such theoretical analyses. [Mus 94]

Most models of the proton center upon the concept of the quark distribution function, *q(x)*, which specifies the probability that the given flavor of quark, q, carries the fraction *x* of the proton's momentum ($x \in [0,1]$). For given processes, such as *ep* scattering, various more useful and reaction−specific derivative functions are defined. These fall into the domains of structure functions, which are usually weighted sums of the distribution functions for all the quark flavors in the proton; and form factors, which determine the gauge couplings of the proton's hadronic current.

Most observables in reactions involving the proton will depend in some way on structure functions or form factors. Reaction cross sections for *ep* processes such as the one occurring in E158 usually depend on Q^2, α^2, and a nuclear form factor, which is also a function of Q^2:

(5) $$\sigma = A\frac{1}{Q^4}\alpha^2 F(Q^2) \quad ,$$

where A is a normalization constant. The parity−violating left−right asymmetry will in turn depend on the Fermi coupling constant, G_F, various kinematic variables, and some form factor specifying the amount of mixing between the elastic and inelastic scattering modes described earlier, the former being insensitive to the proton's compositeness, the latter depending on the internal individual quark current distributions. Since the underlying process ultimately responsible for the observed asymmetry is the electroweak neutral current, the asymmetry will have a $sin^2\theta_W$ term. The elastic scattering of a polarized electron off of a quark is formally similar to electron−electron scattering with respect to the weak mixing angle, modulo the different charge and isospin. The exact Weinberg−angle−dependent fermion couplings are:

e, μ, τ :	Vector: $g_V^f = -1 + 4\,sin^2\vartheta_W$	Axial: $g_A^f = 1$
u, c, t :	Vector: $g_V^f = 1 - \frac{8}{3} sin^2\vartheta_W$	Axial: $g_A^f = -1$
d, s, b :	Vector: $g_V^f = -1 + \frac{4}{3} sin^2\vartheta_W$	Axial: $g_A^f = -1$

As the proton is composed of several quark currents, inelastic scattering will result in a PV asymmetry dependent on a linear combination of weak−mixing angle terms, one for each quark with weights determined by the proton internal structure. Elastic *ep* scattering will also depend on θ_W, with a coupling of :

$$g_V^f = 1 - 4\sin^2\vartheta_W$$

A superposition of the elastic and inelastic contributions, weighted by the relative reaction cross−sections for a given experiment, will then comprise the observed parity−violating asymmetry. Accordingly, the PV asymmetry will have the following form:

$$A_{obs}^{PV} = C\, g_{eff} \quad ,$$

where C is a factor including all the kinematical and non−mixing variables, and g_{eff} is the effective Weinberg−angle dependent coupling, which, following the preceding discussion, will be of the form:

$$g_{eff} = a - b\sin^2\vartheta_W \quad ,$$

where a and b are undetermined constants with one degree of freedom, given the value of the Weinberg angle. The measurement of g_{eff} can then be submitted to the theoretical community as a model−dependent test of some aspects of QCD. Given that the theoretical uncertainties associated with a and b would certainly be greater than those associated with the weak mixing angle, the assumption of an exactly known Weinberg−angle is robust for this purpose. (The angle will be supplied with unprecedented accuracy by E158 as well.) Alternatively, the submission could be framed in the form:

$$A_{ep} = f_{el} A_{el}^{PV} + f_{inel} A_{inel}^{PV} \quad ,$$

where f is the relative cross section of the particular process relative to the total ep scattering cross section. As the elastic asymmetry can be well approximated and the inelastic asymmetry can be bounded above, this formulation of the results provides a more experiment−independent standard of comparison to theoretical results.

2. E158 Experimental Setup

The following is an overview of the E158 experiment, located in End Station A at the Stanford Linear Accelerator Center in Menlo Park, CA.

2.1 Source and Beam

In E158, a beam of polarized 50 GeV electrons is scattered off of an unpolarized liquid hydrogen fixed target. The SLAC accelerator is one of the best sources of high−quality, high energy polarized electron beams in the world. The beam is created optically, when a circularly polarized laser beam impinging on a Gallium−Arsenide cathode ejects polarized electrons into the accelerator. As the experiment attempts to measure left−right asymmetry in Møller scattering, it compares cross−sections of left− and right−polarized pulses separated by the shortest possible period of time, to keep experimental conditions as constant as possible during the two compared pulses. Thus, the experiment rapidly flips the helicity of the electron pulses in a semi−random manner wherein every pulse and the second succeeding pulse have opposite helicity. The two

pulses are compared to compute the left−right asymmetry for the pair. The left−right asymmetry is then averaged over many pulses.

The helicity of the beam is flipped rapidly by Pockels cells at the source. A Pockels cell is an electronically−controlled optical device which polarizes light passing through it according to the applied voltage. The cell has a very short response time and can easily handle 120 Hz operation. Thus, the source laser beam passes through a Pockels cell and its polarization is flipped at the specified rate, which is transmitted to the polarization of the ejected electrons. The electrons are then accelerated to a final energy of 45 or 48 GeV through the 2−mile long SLAC linac by the usual arrangement of Klystron−driven radio−frequency (RF) cavities, and is then directed by bending magnets into End Station A (ESA), where the E158 detector is located. The final beam delivers 250 ns pulses of 6×10^{11} electrons per pulse at 30−120 Hz, with a polarization of about 80%.

2.2 Beam Monitoring and Control

The beam is monitored by a series of beam toroid monitors and beam−position−monitors (BPM's) that measure beam characteristics from which energy, intensity (charge per pulse), and position and angle in the x− and y− directions are computed. (z is the direction of the forward beam momentum.) The toroids simply measure changes in magnetic flux due to the passage of beam electrons through the toroidal wire arrangement. The BPM's are resonant cavities, with resonance conditions set up to be

sensitive to a particular beam parameter. A feedback system from these devices is then used to control the beam and adjust its position to the desired specifications. The beam parameters measured are also crucial in determining false asymmetry components in the measured reaction asymmetry due to left−right asymmetries in the beam parameters themselves. These false beam asymmetries must be removed from the measured asymmetry to determine the true parity−violating physics asymmetry.

2.3 Target

The beam impinges on the target in End Station A. A schematic of the ESA complex is provided in Figure 3. The physics data production target is a 25−liter liquid hydrogen tank 1.5 m in length. It is operated at a temperature of 20 K and pressure of 30 psi. The refrigeration system has a power capacity of 700 W. At a density of 0.07 g/cm^3, the reaction cross−section is large enough to produce enough data for the proposed precision of measurement. Other targets are used for auxiliary measurements. Thus, a polarized iron foil target and a carbon target are moved in to measure beam polarization, linearity of the detector electronics, experiment backgrounds, and other parameters necessary for correcting the measured asymmetry for systematic effects.

2.4 Spectrometer

Most of the beam passes through the target without any significant scattering and passes through ESA to the beam dump. Some beam electrons are scattered through

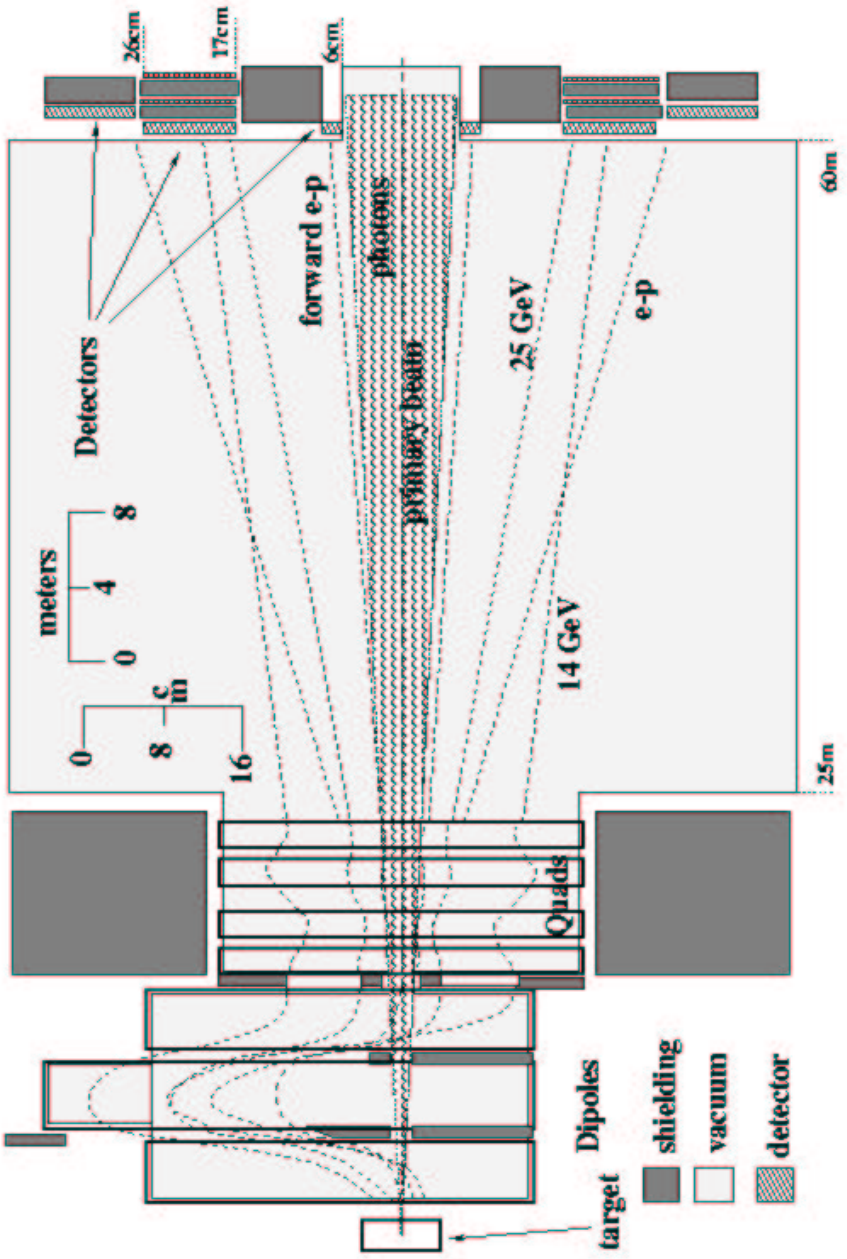

Figure 3. A cross−sectional schematic of End Station A

Møller scattering off of the target electrons and some are scattered from the target protons through *ep* scattering. The electrons scattered off the target at scattering angles of 3−9 miliradians are the particles of interest. The spectrometer is designed to separate

these electrons from the experimental backgrounds and focus them onto the detector, directing the Møller and *ep* electrons into different detector regions.

One of the main backgrounds is bremsstrahlung photons. This background is diminished by a system of three dipole magnets and collimators dubbed the chicane, after the word "chicanery", which signifies trickery. The dipoles bend the scattered electrons and direct them through narrow acceptance windows in collimators situated between the magnets. (The acceptance window is the aforementioned 3−9 miliradians scattering angle range.) Then, they bend them back to their original paths. Thus, the dipoles do not ultimately change the final paths of the electrons. Unlike the electrons, the photons radiated from the target, having no charge, are not bent by the dipoles at all, and thus miss the acceptance windows of the collimators and are stopped by them. The process is a chicanery, since the electrons' post−chicane path is unaffected, but the process does remove unwanted background photons. Hence, the chicane "tricks" the scattered particles and selects only the electrons.

Following the chicane is an array of four quadrupole magnets, which separates the two main scattering signals, the Møller electrons and the *ep* electrons, and focuses them onto separate regions of the detector. The result is a double−peaked radial distribution of the scattered signal, with a Møller peak in the radial regime of 15−25 cm from the *z*−axis at the target, and an *ep* peak between 25 and 35 cm from the *z*−axis at the target. (Figure 4) During *ep* scattering, the electron does not lose much energy since the proton's mass is three orders of magnitude greater than the electron mass. Thus, scattered *ep* electrons are highly energetic, with energies of around 50 GeV. To a first approximation, they are unaffected by the quadrupole magnets, so the *ep* peak in [25,

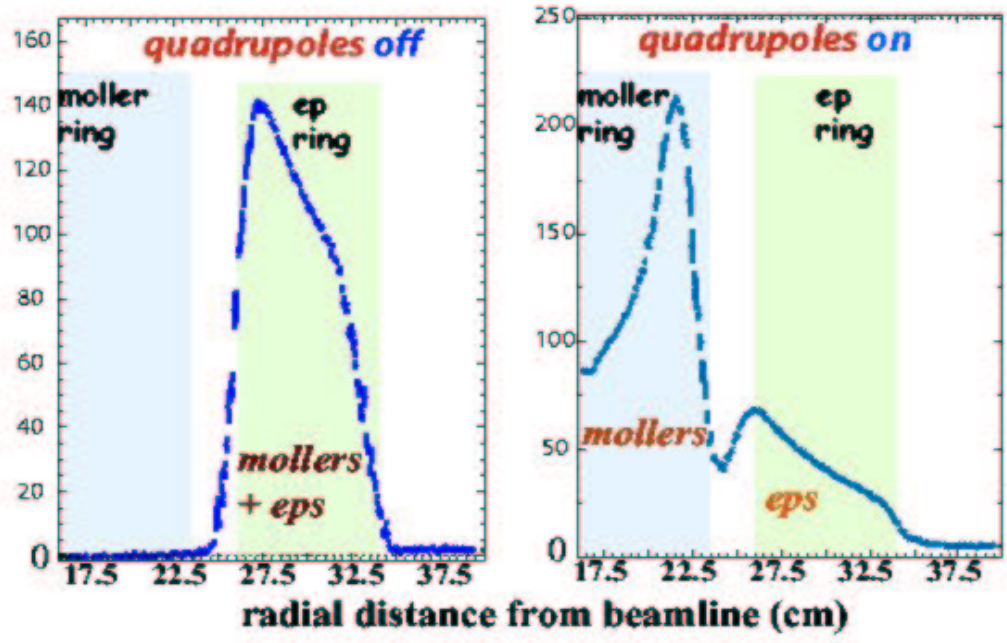

Figure 4. Detector signal versus radial distance from beamline

35]cm corresponds approximately to the original acceptance of 3−9 miliradians. [1] The Møller electrons in the radial acceptance region are far less energetic, and the quadrupoles bend them into the Møller peak.

2.5 Detector

E158 purports to carry out a precision determination of the weak mixing angle by measuring the left−right Møller asymmetry. As such, it is inherently a counting experiment, the operational goal of which is the accumulation of specified statistics and

1The detector is 60 m away from the target along the *z*−axis, so [0.25 / 60, 0.35 / 60] = [0.004, 0.006] ≈ [0.003, 0.009] radians.

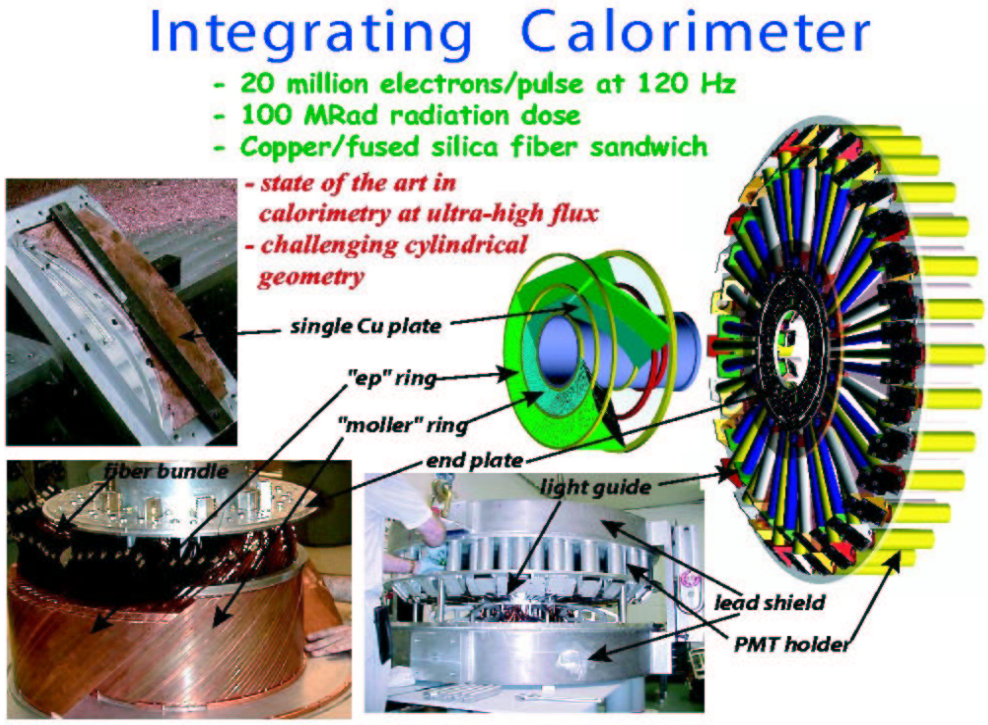

Figure 5. Schematic of the Detector

the understanding and good control of systematic effects contributing false asymmetries to the measured quantity. No particle tracking or identification is required. Instead, the detector must accurately measure the scattered electron flux in a high radiation environment with a low sensitivity to backgrounds. Furthermore, beam parameters must be carefully monitored and controlled, as described in Section 2.3.

The counting of scattered electrons to determine the left−right discrepancy is done by an integrating electron calorimeter, which measures the scattered electron flux over the duration of a pulse. (Fig. 5) The detector is designed to have low response to pions, soft (low−energy) photons, and hadrons; and insignificant response to muons, and heavy ions. This is achieved with a Cherenkov detector design consisting of alternating 3−mm copper plates and quartz fibers. (Fig. 6) The scattered electrons shower in the

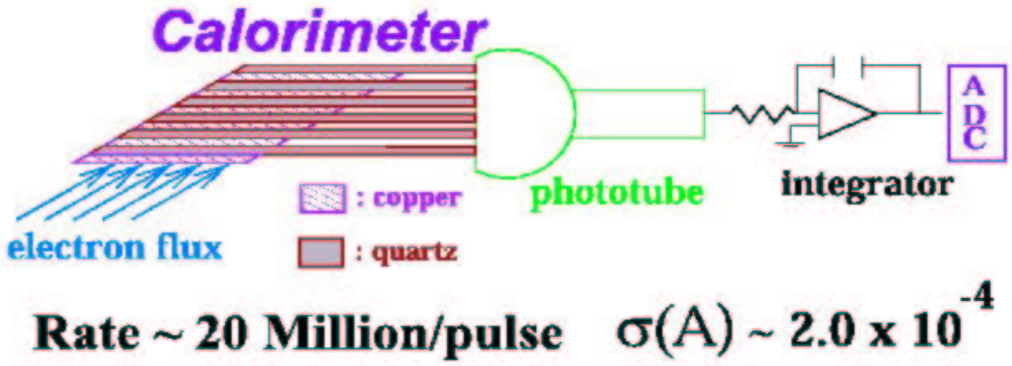

Figure 6. Cherenkov Detection

copper radiator plates, and the resulting avalanches radiate Cherenkov light in the quartz fibers, whose index of refraction is about 1.3. The quartz fibers are oriented at a 45° angle to the direction of the electrons' momentum, so that the Cherenkov radiation is propagated down the fibers through total internal reflection. (Thus, the quartz fibers essentially act as optical fibers.) The Cherenkov radiation is then detected by photomultiplier tubes (PMT's) attached to the end of each bundle of quartz fibers. Thereafter, the signal is processed by discriminators, integrating analog−digital converters (ADC's), and other electronic components, and then sent to the data acquisition system The ADC's have low differential non−linearity (1 least significant bit) and 16−bit precision [ref].

The detector is divided into four concentric, azimuthally symmetric rings, each in turn segmented into several sectors and each sector served by a separate PMT and readout channel. The geometry is centered on the beam line and allows for the detection of any azimuthal dependence of the asymmetry. The rings are, from smallest to largest radius: the *In* ring segmented into 10 channels; the *Mid* and *Out* rings, separated into 20

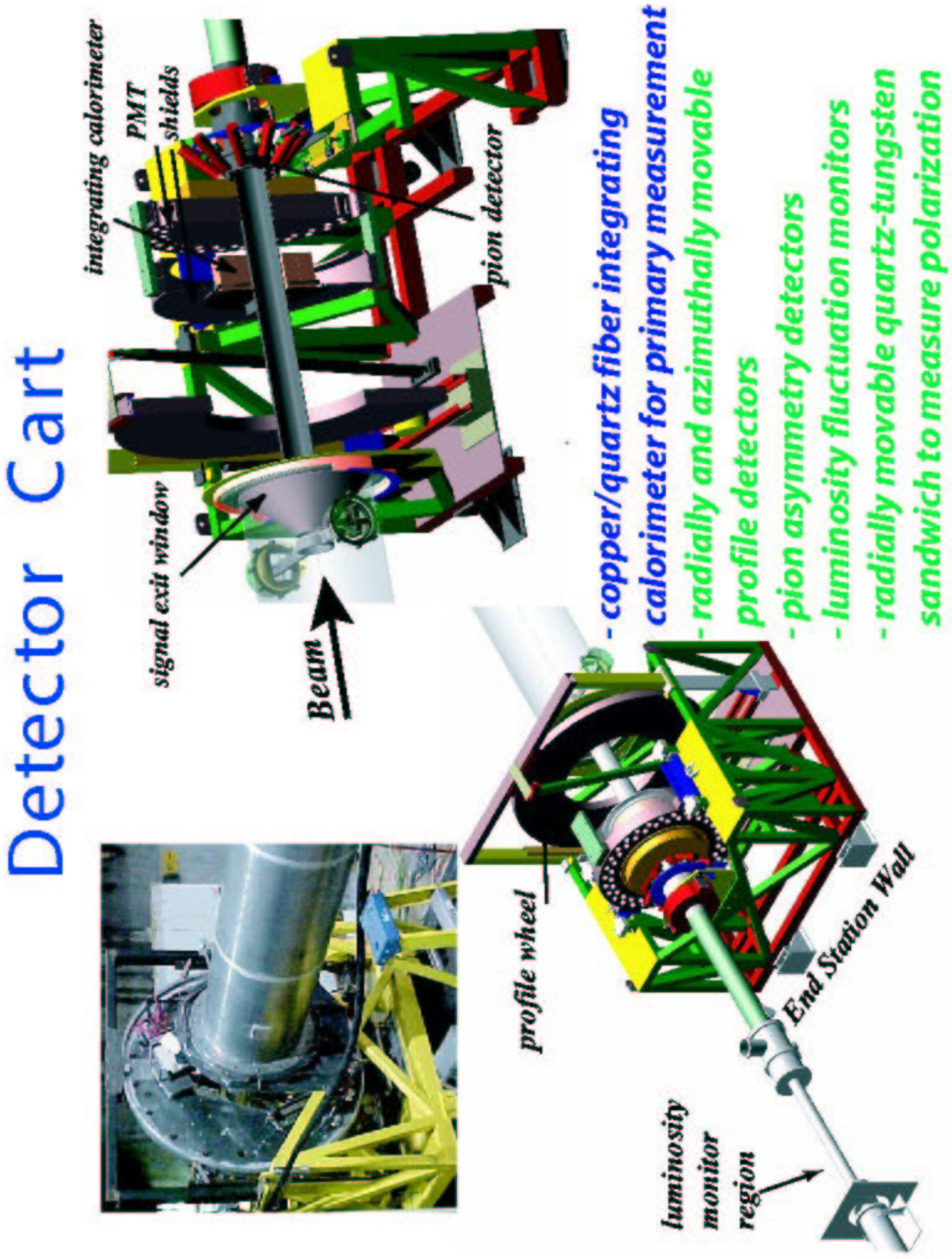

Figure 7. The Detector Complex

channels each; and the *Ep* ring, separated into 10 channels. Since the energy of the scattered electrons depends on the scattering angle, as focused and directed by the spectrometer quadrupoles, each ring is sensitive to a particular energy range. Thus, the *In* through *Out* rings accept most of the Møller peak, while the *Ep* ring accepts most of the high energy 50 GeV *ep* electrons that do not get bent appreciably by the quadrupoles. Naturally, it is primarily from this detector sector that the *ep* parity−violating asymmetry will be extracted.

The detector complex is supplemented by the luminosity monitor, a set of ion−chambers with an Aluminum preradiator hugging the beam pipe right behind the Møller detector. This detector is segmented into 16 channels and is designed to detect very forward−angle *ep* electrons to monitor pulse−to−pulse luminosity fluctuations at the target. Finally, a set of quartz crystals located behind the calorimeter and a few nuclear radiation lengths of absorbers is used to measure the charged pion flux, which is a small background in the experiment. The entire detector complex is depicted in Figure 7.

3. Systematic Corrections

This thesis presents the *ep* asymmetry analysis of the Run I data collected by the E158 experiment in the months of April to June, 2002. The analysis of the raw data involves several steps, an overview of which follows. During the Fall of 2002, this analysis will be repeated on the data set following final reprocessing.

The raw asymmetry recorded by the *ep* channels must be corrected for a variety of systematic effects. First, the asymmetry is corrected for beam asymmetries using regression and the self−consistency of the data is ascertained. Various cuts are then applied based on beam characteristics and the performance of electronics, feedback mechanisms, and the DAQ. The *ep* asymmetry is then adjusted to account for the non−linearity of the PMT's and the imperfect polarization of the beam. Thereafter, a correction is applied to compensate for the effect of the Møller, photon, and pion backgrounds to the *ep* signal. (The photon background is residual bremsstrahlung radiation; the pions are a product of deep inelastic *ep* scattering, for which process the scattered electron is outside the acceptance of the spectrometer and hence not detected). Each background or signal contributes to the measured asymmetry according to the formula:

$$A_{ep}^{obs} = \Sigma\, f_i A_i \ ,$$

where A_i is the left−right asymmetry of the i^{th} signal/background and f_i is the fraction of the total signal from the i^{th} background:

$$f_i = \frac{N_i}{\Sigma\, N_j}$$

The backgrounds with zero left−right asymmetry do contribute to the measured asymmetry by their effect on other signal fractions, f_i. Also, they contribute to the overall systematic measurement error associated with the determination of the signal fractions.

The systematic and statistical errors associated with each of these procedures have to be estimated and propagated to the final asymmetry. Each procedure is described in turn.

3.1 Regression Corrections for Beam Systematics

The first step in correcting the recorded *ep* asymmetry for systematic effects is the correction for beam systematics that contribute false asymmetries to the measured value of the asymmetry. First, the scattering signal from a pulse must be normalized to the intensity of that pulse, as the number of scattered electrons is directly proportional to the intensity. Hence, each pulse signal value is divided by the charge in that pulse. As the final measured quantity is an asymmetry, the division of each signal by the charge will result in the correct unitless asymmetry. This asymmetry is then corrected for false asymmetries from six beam parameters: pulse charge, energy, $x-$position, $y-$position, $x-$angle, and $y-$angle. The observed asymmetry is regressed against the left−right asymmetries or differences of these variables, and the dependencies are then subtracted from the observed value. The procedure is applied separately to every chunk of 2000 events, so that the experimental conditions remain fairly constant over the event range on which the regression is performed. Two alternatives for performing the operation are available: the iterative regression algorithm and the matrix inversion algorithm.

The iterative regression algorithm operates on the simple two dimensional least−squares principle, or χ^2-minimization, iterated over every independent variable. The raw

left−right asymmetry is the dependent variable. The independent variables are, successively, the left−right charge asymmetry (or the asymmetry of beam intensity); and the left−right differences in beam energy, position in the *x* and *y* directions, and angle in the *x* and *y* directions, the *z*−direction being the forward momentum of the beam. The first step is the computation of the arithmetic means of the raw asymmetry and of each independent variable. Next, ($y - \langle y \rangle$) is regressed versus ($x - \langle x \rangle$), where

$$y = \frac{(\frac{N_R}{Q_R}) - (\frac{N_L}{Q_L})}{(\frac{N_R}{Q_R}) + (\frac{N_L}{Q_L})}$$

is the left−right channel asymmetry and *x* the left−right charge asymmetry. (Brackets signify the arithmetic mean.) The regression is done by computing the correlation coefficient

$$b_Q = \frac{\Sigma (y_i - \langle y \rangle)(x_i - \langle x \rangle)}{\Sigma (x_i - \langle x \rangle)(x_i - \langle x \rangle)}$$

Various data cuts are applied in the summation process, wherein data outside of a certain range of the mean in both *x* and *y* are rejected.[2] The correlation is then subtracted from the asymmetry, to produce charge−regressed asymmetry. This is then similarly regressed versus the left−right energy difference, the dependence on which is thereafter likewise subtracted. The algorithm continues successively for every remaining independent variable.

2 The range is usually set in units of the root−mean−squared (RMS) value for each variable. The summation is over events not rejected by the cuts in each chunk of 2000.

The final result is the regressed asymmetry

$$A_{reg} = A_{obs} - \Sigma\, b_i (x_i - < x_i >)$$

which is ideally no longer dependent on any of the independent variables versus which the raw asymmetry was regressed. If desired or necessary, the regression against the six independent variables can then be repeated any number of times until the slopes or widths converge to stable values. This should occur after a few iterations; if not, the data analyst should conclude that non−linear factors are significant and that linear regression is not a suitable procedure for data correction in this case. On the data set used in this analysis, two iterations were enough to produce converged correlation coefficients. Finally, the cut range of the algorithm can be altered to produce better results. (The value for the cuts was two RMS.)

The other regression alternative is the matrix inversion algorithm, which is the standard multivariate χ^2−minimization algorithm. Here, the channel asymmetry, *y*, is regressed in (n+1) − dimensional space versus n independent variables, x_i. The variables are the same as in the iterative algorithm. The formula for the vector of correlation coefficients is

$$B = X^{-1} Y,$$

$$X_{ij} = \Sigma\, (x_i - < x_i >)(x_j - < x_j >), \quad Y_i = \Sigma\, (x_i - < x_i >)(y - < y >)$$

where the upper−case variables are matrices; the indices of upper−case variables refer to the corresponding matrix entry; and the indices of lower−case variables refer to the appropriate independent variable versus which the raw channel asymmetry is regressed.

As with the iterative algorithm, a data cut of two RMS is applied when computing the sums involved and the algorithm is run twice on the asymmetries, which is enough to produce stable values for the correlation coefficients. Currently, the matrix inversion algorithm is the default regression choice, with the iterative regression algorithm preserved as an option to clean up regression residuals left over from the matrix inversion algorithm.

The statistical errors on the coefficients produced by the matrix inversion algorithm are just the appropriate diagonal entries of the X matrix defined above multiplied by the regressed asymmetry. In addition, a source of systematic regression error is the incomplete reliability of linear regression in removing beam dependencies from the raw channel asymmetry. This imperfection results from non−linear dependence of the channel asymmetry on the beam asymmetries and differences. Although the beam dependencies should be very linear, the systematic error due to non−linearities must be estimated. This is done by comparing the regression corrections to the asymmetry with the corrections due to dithering of the beam parameters. Dithering is a process wherein the parameters of the beam are willfully varied by an automated computer program and the correlation between the beam parameters and the channel asymmetries is measured. In principle, the dithering and regression corrections should be statistically identical, as it should not make a difference on the raw asymmetry whether the beam parameters vary through random fluctuations or through artificial control. The inconsistency between the regression and dithering corrections to the channel asymmetry is thus a measure of the lack of reliability of the regression algorithm, which is a measure of the systematic error associated with the procedure. The regression and dithering corrections should be within

statistical error bars or so of each other in order for regression to be reliable at all.

3.2 Consistency Analysis

After regression and associated analysis, the data is tested for experimental consistency. This involves the examination of the behavior of the measured, corrected *ep* asymmetry versus time and azimuth. The asymmetry is thus plotted versus run number and versus *ep* channel. For both cases, the data is fit with a zero degree polynomial, which essentially gives the total asymmetry averaged over time and azimuth, respectively. The chi−squared statistic and associated probability from this fit are a measure of experimental consistency. The probability should be at least a few per cent for the data to be reliable. If the probability is smaller and/or there exist patterns and outliers among the data points, the offending runs should be examined for causes of the deviation. If the deviation is understood and determined to come from abnormal or averse systematic conditions, such as abnormally large beam charge asymmetry, the poor data points can then be confidently removed and the procedure repeated to yield superior consistency statistics. Only when these are acceptable can the analysis proceed. The reprocessing of the data in the Fall of 2002 will implement beam quality cuts and other cuts that should remove all runs that outlie due to systematic abnormalities.

3.3 PMT non−linearity

The next correction involves the estimation of non−linear effects in the photomultiplier tubes used to detect the signal. The non−linearity affects the scaling of the PMT output with the electron signal input. At large input signals, the response from the PMT is below the linear extrapolation from the input/output scaling at low input signals, where the PMT is linear. This reflects a negative quadratic component in the response characteristic that in turn affects the measured asymmetry. (Higher order responses are assumed to be negligible.)

Ignoring higher order effects, the PMT output signal is

$$P = \epsilon_0 N - \epsilon' N^2$$

where ϵ_0 is the linear PMT response, ϵ' is the negative quadratic response (also a function of *N*), and *N* is the size of the input signal to the PMT. Defining

$$\alpha = \frac{\epsilon'}{\epsilon_0} N$$

we get:

$$P = \epsilon_0 N (1-\alpha)$$

Assuming that $N_L \simeq N_R \simeq N$, where *N* is the average left−right signal, the measured asymmetry and true parity−violating asymmetries are:

$$A_{PV} = \frac{N_R - N_L}{N_R + N_L}$$

$$A_{obs} = \frac{\epsilon_0 N_R (1 - \alpha \frac{N_R}{N}) - \epsilon_0 N_L (1 - \alpha \frac{N_L}{N})}{\epsilon_0 N_R (1 - \alpha \frac{N_R}{N}) + \epsilon_0 N_L (1 - \alpha \frac{N_L}{N})}$$

Carrying out appropriate Taylor expansions in α and ignoring terms quadratic in α, we get:

$$A_{obs} = A_{PV}(1 - \alpha)$$

Thus, estimating the parameter α at a given signal size produces the effect of the PMT non−linearity on the measured asymmetry. This effect can be estimated in bench studies or *in situ* from experimental data.

In situ measurements are the most accurate method for determining PMT non−linearity, as they provide a determination within experimental conditions closest to the physics production setup. The method again involves the iron foil, and centers upon the comparison of asymmetries and signals for runs with the iron foil and target in versus runs with just the iron foil in, *sans* target. This is possible since the PMT input in iron−foil−only runs is very small, located in an input signal regime where the PMT is almost totally linear. Using the above definitions for output PMT signal and measured asymmetries, we get

$$(1 - 2\alpha) = \frac{A_{Fe+Target}}{A_{Fe}} \frac{P_{Fe+Target}}{P_{Fe}}$$

where the asymmetries are observed (not true) asymmetries. Thus, the non−linearity parameter can be measured for any target, with $(1-2\alpha)$ becoming progressively smaller as the target radiation length increases (the hydrogen target having the most radiation lengths, and thus generating the largest non−linearity corrections). The non−linearity is measured for each channel separately, and then averaged over all channels to determine the total non−linearity that is used to correct the measured asymmetry.

Although the *in situ* methodology is the preferred technique for linearity studies, the method is currently not completely understood. Alternate methods are being explored for *in situ* estimation of the PMT linearity; they will be used to correct the Møller asymmetry. For this thesis, the results of simple bench studies of the PMT non−linearity will be used. The methodology gains accuracy through the low non−linearities of the PMT's at the low signal levels of the *ep* region.

3.4 Polarization Correction

The final step in the analysis is the correction for the incomplete polarization of the linac beam delivered to End Station A. This correction can be performed last, as the incomplete polarization is a simple dilution effect that affects every measured quantity in the experiment equally. Thus,

$$A_{obs}^{corrected} = f_{pol}\, A_{ep}^{true}$$

where f_{pol} is the polarization fraction. As usual, the error on the polarization fraction of the beam must be propagated to the final asymmetry.

The polarization per cent is measured using a polarimeter setup involving the

polarized iron foil without the hydrogen target. The process is then the scattering of a polarized beam from a polarized foil. (No unpolarized target is present.) The scattered signal is proportional to the polarization of the beam and the polarization of the foil, which is known as the iron is magnetized to saturation. Hence, the polarization of the beam can be accurately determined and used to obtain the true parity−violating *ep* asymmetry.

3.5 Møller Background

Although the electrons produced through Møller scattering are focused into a Møller peak detected by the *In* through *Out* detector rings, some Møller electrons do leak into the *Ep* detector ring. These form a background to the *ep* signal and decrease the measured asymmetry, as the Møller asymmetry is a factor of 10 smaller than the *ep* asymmetry. Since this underestimates the *ep* asymmetry, the size of the Møller signal in the *Ep* region must be estimated and the measured asymmetry corrected for the Møller pollution. This is done by examining the data from runs taken with the iron foil.

The iron foil is a thin sheet of iron inserted close to the target and polarized by a set of Helmholtz coils. The electrons scattered off of the iron foil result in a large detected left−right asymmetry, on the order of 5%. If the hydrogen target is in, this decreases the measured asymmetry to about *500 ppm*. Moreover, virtually the entire value of the asymmetry is from Møller scattering, as *ep* electrons are unaffected by the

polarization of the foil, since magnetization does not affect the proton (or any nucleus).[3] While the asymmetry is considerably different from the asymmetry in normal production conditions with no iron foil, the ratio of the *ep* signal to the Møller signal is not significantly altered, since the hydrogen target remains in and the iron foil contributes a negligible radiation length. Thus, the signal size remains similar to production conditions. Hence, the large left−right asymmetry in the *Ep* detector measured with the foil inserted yields the fraction of the measured *ep* signal due to Møller electrons spilling into the *ep* region according to this formula:

$$A^{obs}_{ep,Fe} = A_{ee,Fe}\frac{N_{ee}}{N_{ee}+N_{ep}+N_{bkgd}}$$

where, $A_{ee,\,Fe}$ is the polarized iron Møller asymmetry, as measured in the Møller portion of the detector with the iron foil inserted; $A^{obs}{}_{ep,\,Fe}$ is the asymmetry measured in the *Ep* region with the iron foil inserted; and N_i is the signal contribution from the i^{th} component signal detected in the *Ep* region (N_{bkgd} signifying additional backgrounds besides the Møller signal). Thus,

$$f_{ee} \equiv \frac{N_{ee}}{N_{ee}+N_{ep}+N_{bkgd}} = \frac{A^{obs}_{ep,Fe}}{A_{ee,Fe}}$$

3.5 Other Experimental Backgrounds

3 In other words, because its mass is 2000 times greater than that of the electron, resulting in a much smaller proton magneton, it is impossible to polarize protons or nuclei with available magnetic fields, and the *ep* electrons thus behave as if they have scattered from an effectively unpolarized target. Hence, their left−right asymmetry is negligible when compared with the polarized Møller asymmetry. The asymmetries from the other backgrounds are similarly dwarfed by the Møller iron asymmetry.

There are two other major experimental backgrounds: bremsstrahlung photons and pions. Although the photon background has no left−right asymmetry, its presence does dilute the *ep* asymmetry in the measured value by decreasing the fraction of the true *ep* signal detected in the *Ep* ring. More importantly, the error on its measurement contributes to the error on the determined *ep* asymmetry.

To estimate the photon background, one analyzes the runs taken with the quadrupole magnets turned off. With the quads off, all the scattered electrons travel according to their original scattering angle within the 3 to 9 miliradian acceptance region, which as discussed before corresponds to the *Ep* detector ring at the detector position (60 m downbeam from the target). Hence, the Møller region of the detector (*In* through *Out* rings) does not receive any scattered electrons with the quadrupoles off. However, its photonic background is the same as with the quadrupoles off, since photons are not affected by magnetic fields. Moreover, the functional dependence of the photonic background versus radius is decreasing and, to a good approximation, flat over the *Out* and *Ep* regions. Hence, by measuring the photon signal in the *Out* detector with the quadrupoles off, we get a good estimate of the size of the quad−on (equal to quad−off) photon background in the *Ep* region as well. Any error would be an overestimation of the photonic background, so the approximation is actually a conservative one (the larger a background is, the larger the error on the parity−violating *ep* asymmetry propagated from the background becomes). Using this method, the photon background fraction of the total signal in the *Ep* region is

$$f_{\gamma}^{ep} = \frac{f_{\gamma}^{out} P_{out}}{P_{ep}}$$

where *P* is the normal, quads−on production signal in the appropriate detector region. Alternatively, for a more precise determination of the background, the numerator of the above expression can instead be the extrapolation to the *Ep* region of the functional dependence of the quads−off signal versus radius obtained from all the Møller detector rings. As mentioned before, this functional dependence is fairly flat beyond the *Mid* ring, so this added precision would not be great.

This procedure will not be performed until the Quads Off data is properly understood. This omission is allowable, as the relative photon effect on the *ep* asymmetry is negligible due to the asymmetry's large value (*~1 ppm*). Hence, this analysis treats the photon background as a systematic error, rather than as a correction.

The pion background consists of pions produced in deep inelastic scattering of the electron off the proton. Unlike in shallow inelastic scattering, in deep inelastic scattering the electron does lose a significant fraction of its energy, which is transferred to the emitted pion. The electron scatters at very large angles, and thus is not captured in the acceptance window. The emitted pions, however, contribute a 0.1% background in the acceptance window, which is measured directly by the pion scintillator. The pion background has a non−zero left−right asymmetry. Hence, it has both a dilution effect on the *ep* signal and a direct asymmetry contribution to the measured *ep* asymmetry.

4. Results

The data is divided according to energy, as the *ep* asymmetry is proportional to

Q^2, which is in turn proportional to beam energy. Thus, the data are divided into 48 GeV and 45 GeV samples.

4.1 Regression Corrections for Beam Systematics

Figures 8−9 shows the regression correction versus time averaged over the six beam parameters. Figures 10−11 show analogous results for the dithering process. The total regression correction to the measured asymmetry for the entire data set was computed to be (1.1 ± 3.0) *ppb* (parts per billion) for 48 GeV; and (−8.7 ± 3.8) *ppb* for 45 GeV. The corresponding quantity for dithering was computed to be (3.54 ± 14.43) *ppb* for 48 GeV and (−4.18 ± 15.39) *ppb* for 45 GeV. The two measurements agree within one sigma error bars. However, the results are entirely dominated by the large error on the dithering measurements. Hence, the dithering errors are assigned as a systematic error on the regression methodology.

4.2 Consistency Analysis

Figures 12−13 display the regressed asymmetry versus time (run number). The zero−degree polynomial fit and associated statistics are also displayed. P0 indicates the value of the best−fit asymmetry and error.

Despite a couple of outlying runs, the data appear to behave well with respect to

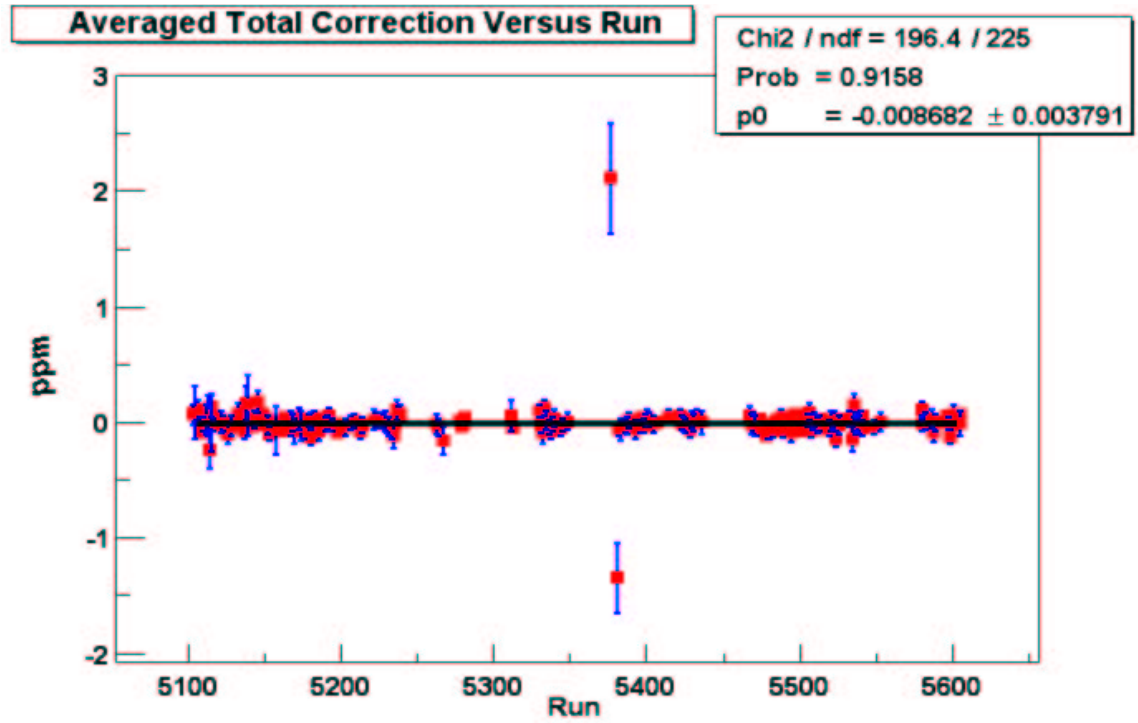

Figure 8. 45 GeV, Regression Corrections

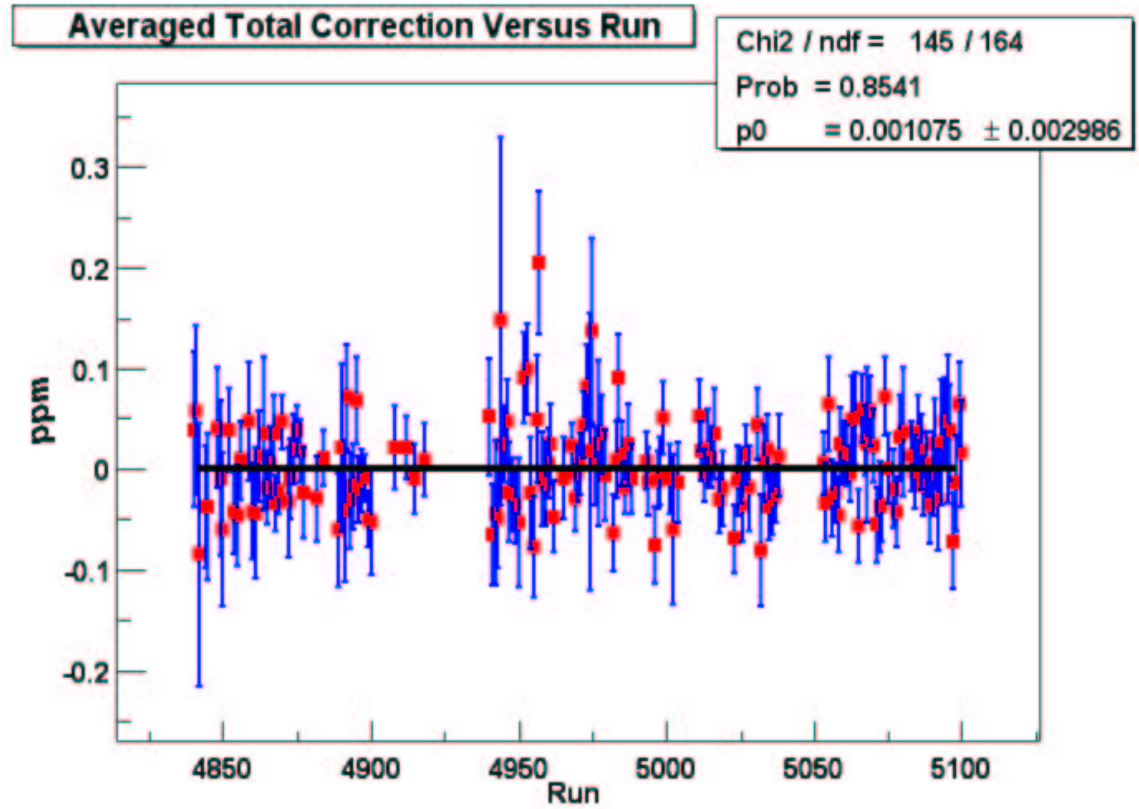

Figure 9. 48 GeV, Regression Corrections

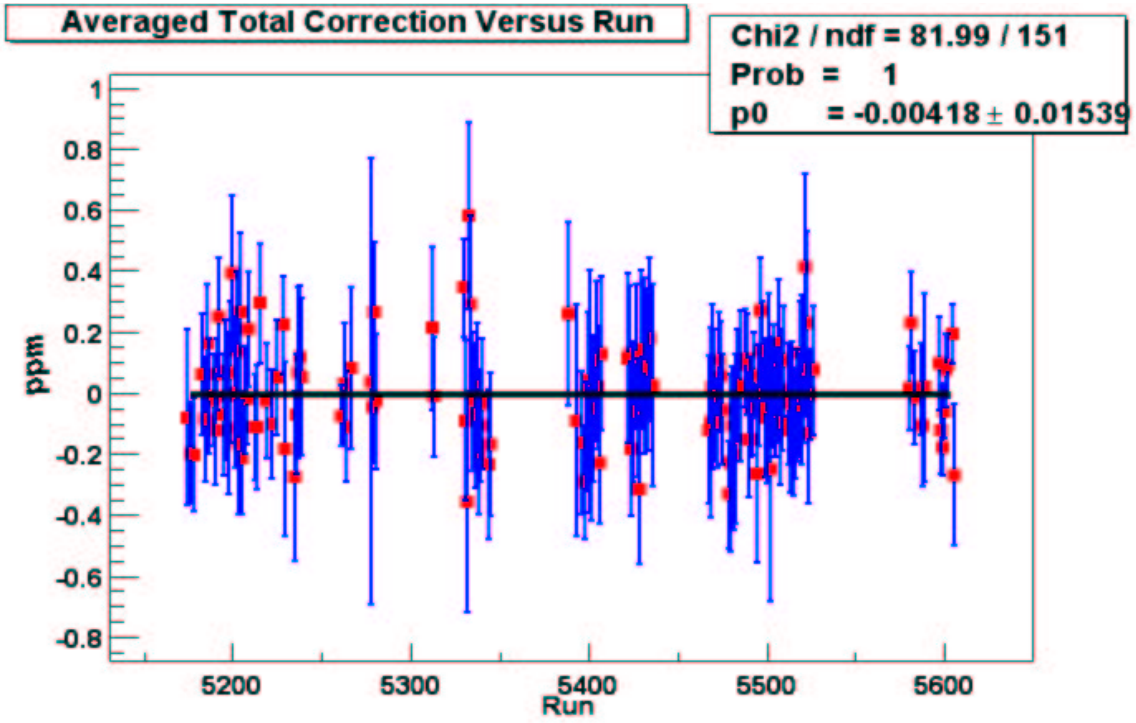

Figure 10. 45 GeV, Dithering Corrections

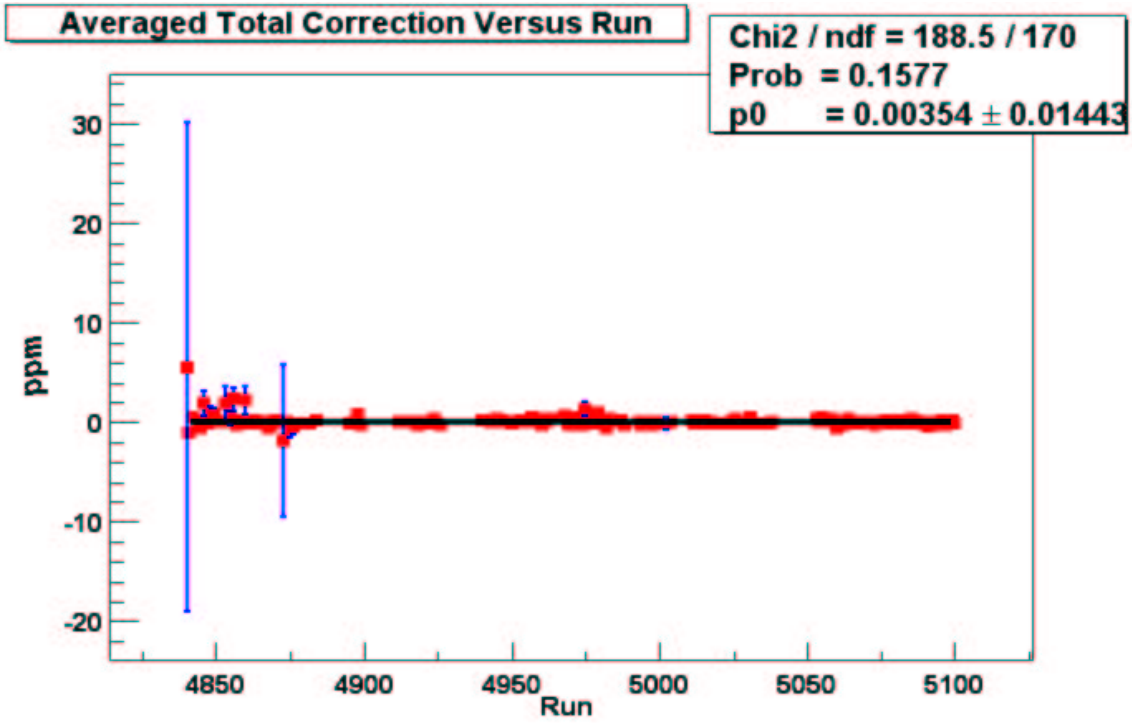

Figure 11. 48 GeV, Dithering Corrections

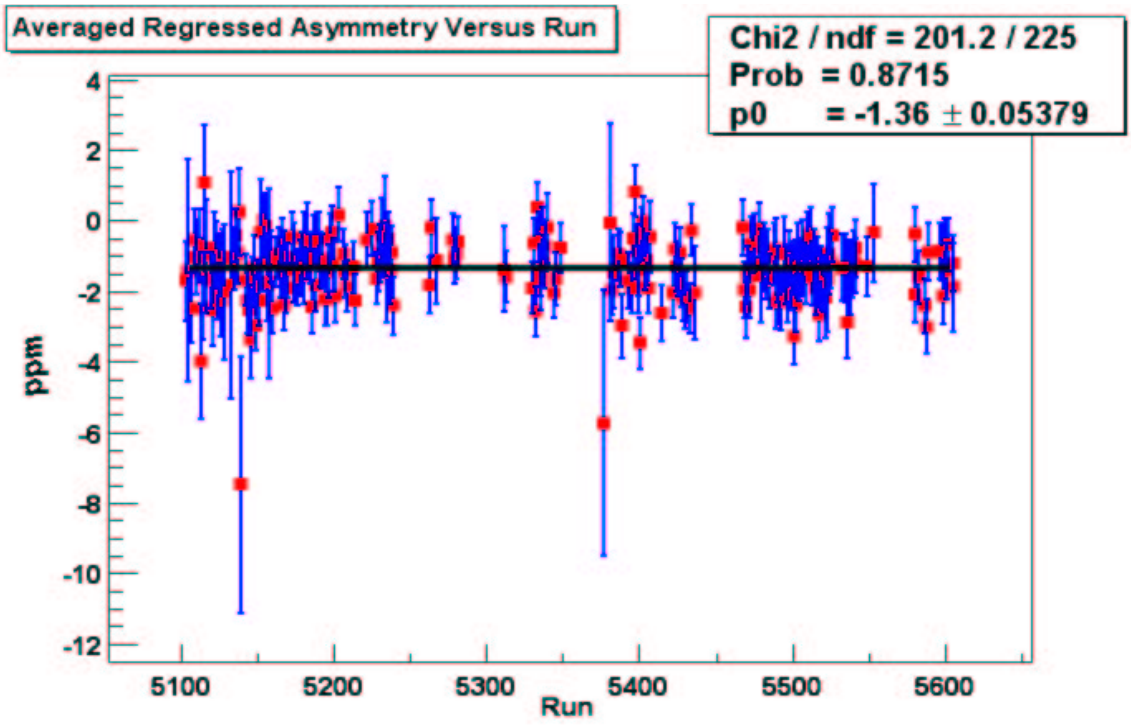

Figure 12. 45 GeV

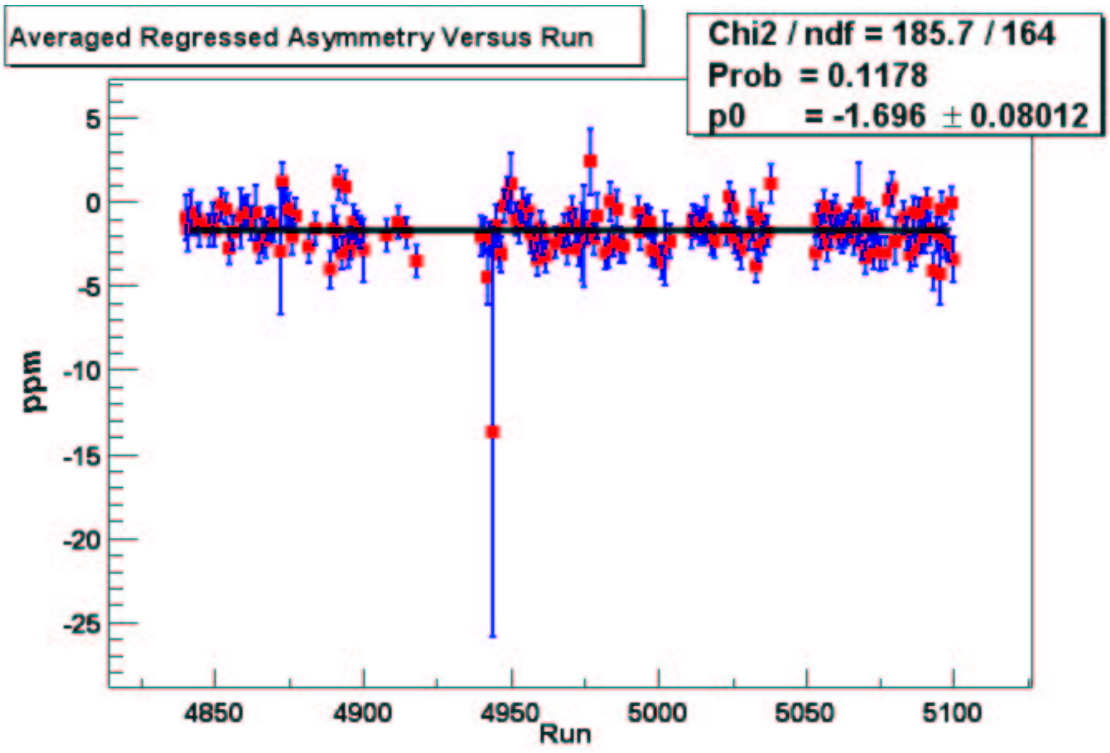

Figure 13. 48 GeV

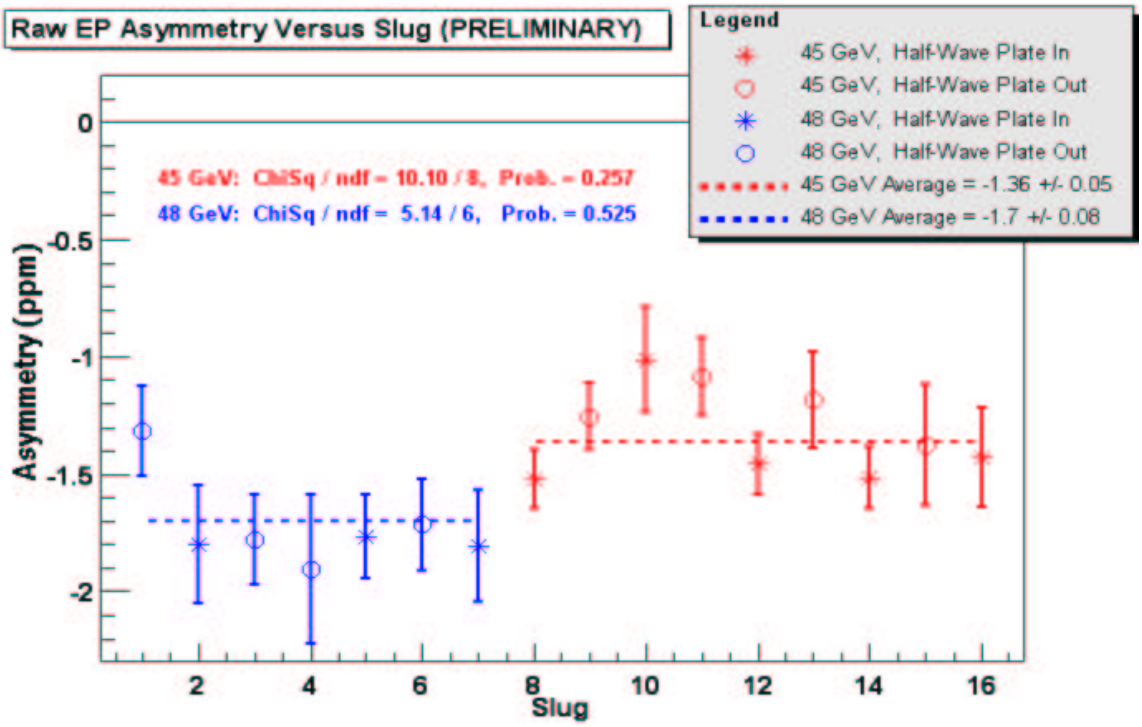

Figure 14. Consistency Versus Time

time, the probability of consistency from the fit being 12% and 87% for the 48 GeV and 45 GeV samples, respectively. Figure 14 and Table 1 also show the behavior of the asymmetry versus Wave Plate, which is inserted at the source to test experimental consistency. Again, the data pass the consistency requirement and the asymmetry passed on to the next step of the analysis is (1.36 ± .05) *ppm* for 45 GeV and (1.70 ± .08) *ppm* for 48 GeV.

Energy, GeV; Wave Plate Status	***Asymmetry, ppm***	χ^2 ***/ ndf***	***Probability, %***
48, Out	−1.635 ± .1045	98.66 / 99	49.56
48,In	−1.784 ± .1249	86.15 / 64	3.16
45, Out	−1.205 ± .08995	54.18 / 74	95.97
45, In	−1.447 ± .06712	142.4 / 150	65.89

Table 1. Consistency Analysis

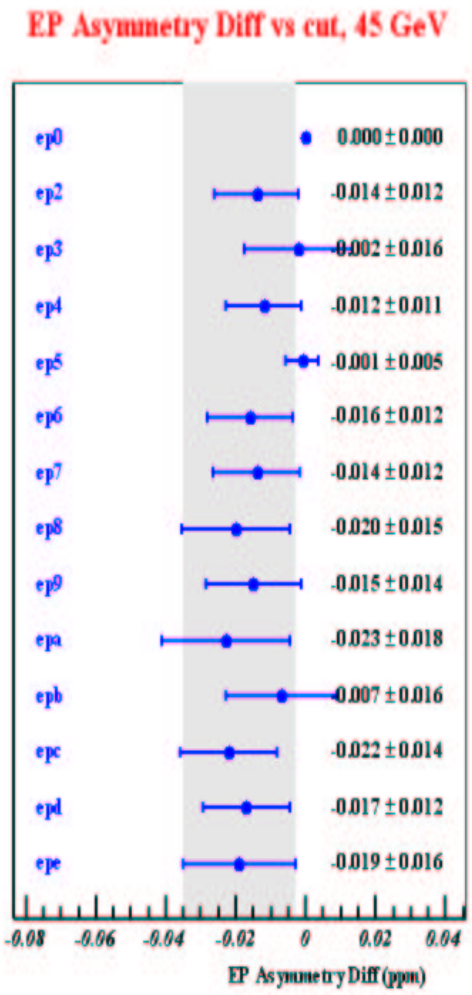

Figure 15

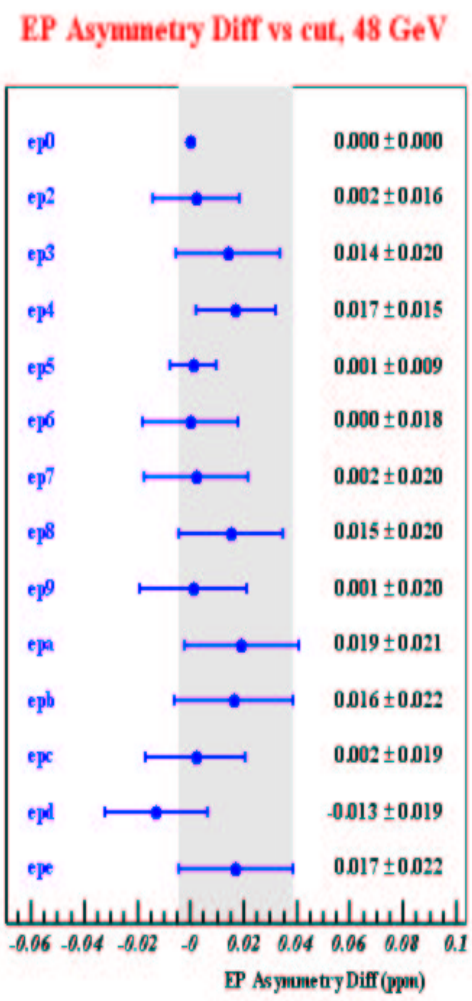

Figure 16

The data were also analyzed for consistency versus different beam cut and electronic cut combinations. Figures 15−16 shows the differences and associated errors of the cut combinations with reference to the loosest cut combination. The data is well−behaved, and a conservative cut consistency systematic error of 22 *ppb* and 23 *ppb* is assigned to the 48 GeV and 45 GeV data samples, respectively. Finally, Figures 17−18 show asymmetry pulls by run as a final check of consistency.

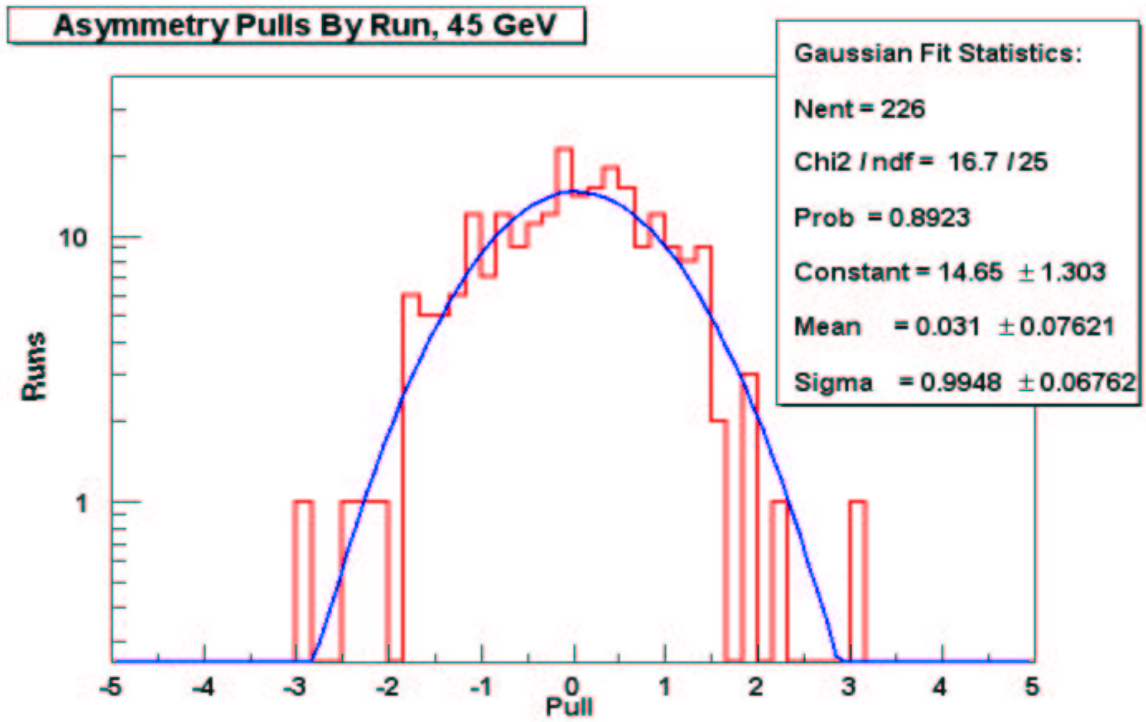

Figure 17

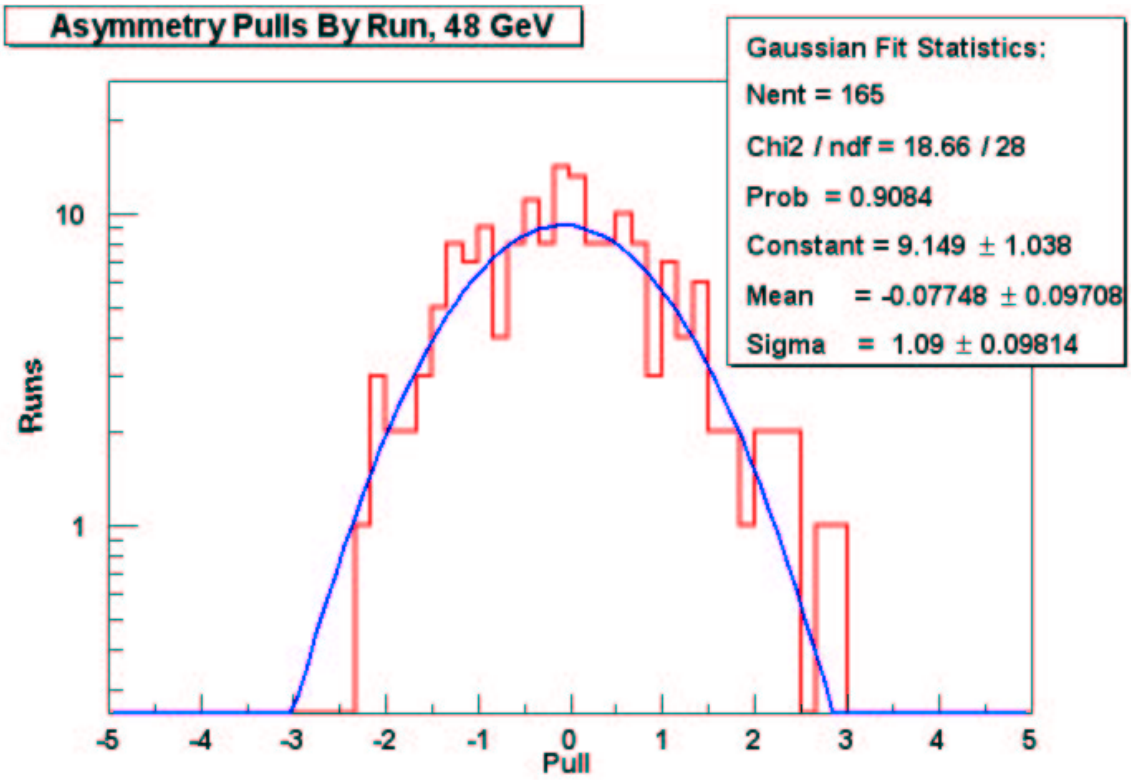

Figure 18

4.3 Backgrounds, Non−linearity, and Polarization

An estimate of the Møller background signal fraction in the *Ep* region is 0.027 ± 0.004, or about 3%. Figure ____ shows the iron and hydrogen data used to determine this estimation. A conservative theoretical estimate of the Møller asymmetry is −320 ppb at tree level multiplied by .6 to account for radiative corrections. A conservative systematic error of 1% is assigned for the photon background. The pion background is estimated as follows:

The pion particle rate is 1% of the Møller rate (upper limit). In the calorimeter, pions deposit approximately 1 / 3 of their energy, which is in turn a factor of 2 lower than the Møller energy. Hence, pions deposit 1 / 6 % of the total energy seen in the Møller detector. The ratio of the energy deposited in the *ep* detector to that in the Møller detector is about 0.4, as approximated from the ratio of the Quads−On to Quads−Off signals. Thus, the pions deposit (1 / 6) / 0.4 = 0.4 % of the total energy seen in the *ep* detector. The pion asymmetry is 2 ppm (upper limit). Therefore, the upper limit on the pion contribution to the measured ep asymmetry is (0.004)(2) ppm = 8 ppb. Accordingly, a conservative systematic error of 20 *ppb* is assigned from the pion background to the measured *ep* asymmetry.

Based on bench studies, the average linearity of the PMT's used in the *Ep* ring is

$$(1-\alpha) = 0.99 \pm 0.05$$

Finally, the polarization of the beam is estimated to be 85% ± 5%.

Using these very preliminary estimates, the estimated true physical parity−violating *ep* asymmetry is

$$A_{ep}^{PV}(45\,GeV) = (-1.66 \pm 0.07\,(stat) \pm 0.14\,(syst))\ ppm$$
$$A_{ep}^{PV}(48\,GeV) = (-2.07 \pm 0.10\,(stat) \pm 0.17\,(syst))\ ppm$$

$$\frac{A_{ep}^{PV}(48\,GeV)}{A_{ep}^{PV}(45\,GeV)} = 1.25 \pm 0.08\,(stat) \pm 0.03\,(syst)$$

5. Conclusion

This thesis has presented the *ep* asymmetry analysis of the Run I data produced by the E158 experiment. As the raw experimental data set has not been processed fully and some systematic studies have not been completed, some of the *in situ* stages of systematic investigation had to be replaced by alternate or theoretical estimates, which increased significantly the systematic error of the final measurement. The analysis was thus systematics−dominated, with the primary source of error being non−linearity of the PMT's and beam polarization. Hence, the analysis will await the improved measurements of these quantities before finalizing its systematic study to yield the definite *ep* parity−violating asymmetry. This should occur sometime in the Fall of 2002.

While not definite, the measurement is still currently the most relatively precise determination of a parity−violating asymmetry. Moreover, the analysis has been invaluable as a study and implementation of methodology. It has demonstrated the consistency of the regression algorithm used in the experiment, as well as showing its

small effect on the total systematic error. Furthermore, it ascertained the consistency of the data sample, as well as yielding standardized procedures and software for the task and identifying the primary sources of systematic error. Finally, as the produced value of the *ep* asymmetry proved to be larger than expected, the E158 collaboration decided to install collimators to block the *ep* electrons during Run II of the experiment (Fall 2002, 2003). This should reduce the systematic error on the Møller asymmetry from the *ep* background to below 20 *ppb* in that Run.

The resulting structure is a tested methodological program, which can be iteratively applied to the reprocessed data sample that will soon be available. Therefore, this investigation will be the machinery used to determine and characterize the *ep* parity−violating asymmetry with the level of statistical and systematic confidence of 7−9 sigma.

Acknowledgments

I would like to express my warm gratitude to Yury Kolomensky, who is directly responsible for most of my exposure to active physics research, and who has been the primary motivator and resource in the progression of my career outside of the classroom for the last year and a half. Thanks are also extended to Brock Tweedie, whose advice and companionship in 317 LeConte have helped me navigate the world of senior−year physics. Of course, the entire E158 collaboration has my greatest gratitude as well, for their general contribution to the experiment, which benefits all, and for the personal help that they have given me. Finally, the helpful staff of the Physics Department of UC Berkeley has eased tremendously the formal aspects of obtaining a physics degree, for which feat I acknowledge them as well.

References

[Der 79] E. Derman and W. J. Marciano, Ann. Phys. **121**, 147 (1979).

[Gla 70] S.L. Glashow, J. Iliopoulos and L. Maiani, Phys. Rev. D 2 (1970) 1285.

[Lep 01] Delphi Collaboration, "Measurement of the W Boson mass and width in DELPHI at LEP," Int.J.Mod.Phys.A16S1A:284−286,2001.

[Lep 93] Working Group on LEP Energy (L. Arnaudon et al.), "Measurement of the mass of the Z Boson and the energy calibration of LEP," Phys.Lett.B307:187−193,1993.

[Mus 94] M. J. Musolf, et al., Phys. Reports. **239**, 1−178 (1994).

[NuT 01] see S. Davidson et al., "Old and new physics interpretation of the NuTeV Anomaly," JHEP 0202:037,2002 .

[Sal 68] A. Salam, in: Elementary Particle Physics, ed. N. Svartholm (Almquist and Wiksell, Stockholm, 1968) p. 367.

[Wei 67] S. Weinberg, Phys. Rev. Lett. 19 (1967) 1264.

[Woods 95] see M. Woods, "Review of weak mixing angle results at SLC and LEP," presented at the International Europhysics Conference on High Energy Physics, Brussels, Belgium, July 27−August 2, 1995.